Theoretical Model of the Densification During Hot Pressing and its Verification

Edwin Gevorkyan[1] , Miroslaw Rucki[2(✉)] , Volodymyr Nerubatskyi[1] ,
Zbigniew Siemiatkowski[2] , Dmitrij Morozow[2] , and Hanna Komarova[1]

[1] Ukrainian State University of Railway Transport, Kharkiv, Ukraine
[2] Kazimierz Pułaski University of Technology and Humanities in Radom, Radom, Poland
m.rucki@uthrad.pl

Abstract. In the paper, theoretical model of the densification process was proposed for the sintering under pressure and directly applied electric current. Despite the wide application of sintering processes in industry, it is still discussed what mechanisms are responsible for densification and how to predict the properties of the sintered material. In this paper, the model was proposed based on summation of the partial densities obtained for the given temperature and pressure from plastic deformation, diffusion, power law creep, Nabarro-Herring creep during the process duration time. The process itself was divided to two stages, before the relative density 0.9 is reached, and after it. Initial experimental results proved satisfactory conformity with the model below 10%.

Keywords: Densification · Sintering · Hot-pressing · Creep · Model

1 Introduction

In a powder metallurgy, full density processing techniques based on hot pressing are widely applied. A group of novel consolidation techniques that combine the advantages of vacuum sintering and hot pressing include pressure-assisted densification and unique benefits from the direct application of electric current [1]. In general, electroconsolidation is advantageous because of the lower sintering temperature, higher heating rate, and shorter sintering time than that of other sintering techniques. Electrical field has certain effects on mass transport, reactivity, diffusion, grain boundary mobility and other processes that take place during compaction of the powder [2]. However, there are some difficulties with modeling of the process, since early presumptions on the role of plasma and discharge phenomena in the field assisted sintering, that even resulted in designation "spark plasma sintering," was probably wrong [3].

Other problem with theoretical description of the densification is related to the dimensions of particles. The sintering mechanism in the case of micrometer-sized particles is well studied and many papers have been published, while the sintering of submicron powders has its own specifics, where micromechanistic models for densification are not applicable [4]. Despite variety of the theoretical explanations, there is no comprehensive model that would describe the entire process.

In the current research, theoretical model for the hot-pressing under directly applied electrical current is proposed. Material of the simulations and experiments was chosen aluminum oxide (Al_2O_3), since it is "one of the most important ceramic materials and its dense nanocrystalline form (with <100 nm grain size) is of great scientific and technological interest" [5]. Densely sintered alumina exhibit outstanding wear resistance and strength, valuable in many mechanical applications [6], as well as nanoporous alumina-based ceramics [7]. Thus, the investigations were aimed at finding reliable theoretical model useful also for submicron alumina powders.

2   Theoretical Model

2.1   General Assumptions

Model of the hot-pressing consolidation under directly applied electrical current of 50 Hz was based on the classical theory described in the works by Ashby and co-authors [8, 9]. Essentially, the model assumes possibility of simultaneous processes of plastic deformation, power law creep, Nabarro-Herring creep, as well as mass transfer as a result of grain-boundary diffusion and surface diffusion. The powder was described as a set of spherical particles of similar diameters [10], randomly compacted. Theoretically, if the sample was fully compacted with no pores, the bulk density ρ would be reached. Since the pores are not fully eliminated, the relative density D_R of the sample is smaller than 1. It is usually convenient to distinguish between three stages of sintering, namely initial, intermediate and final ones [11]. However, in the present model, it was useful to divide the densification process to two stages only: first stage covered relative density D_R from the loose powder initial density D_{R0} up to $D_R = 0.9$, while the second stage dealt with relative densities $0.9 < D_R < 1.0$. The densification was understood as a decrease of the overall volume due to shrinkage of the distances between particles and, thus, was modeled as increase of the single particle radiuses around fixed centers. Number of contacts between a single particle and other particles is calculated, and then mean contact surface, radius of the neck surface is determined to find the effective pressured in each contact point. In the second stage, the surface of a particle takes form of a polyhedron and the effective pressure decreases because of inner pressure of the pores concentrated in the corners of the polyhedrons.

The relative density was determined through summation of the partial densities obtained for the given temperature and pressure from plastic deformation, diffusion, power law creep, Nabarro-Herring creep during the process duration time.

As a result, it was possible to plot the diagrams of hot-pressing, i.e. dependence between the relative density D_R and process parameters (pressure, temperature, time). The subjects of investigation were powders of alumina of average particle diameters 0.6 μm. Next, series of experiments were performed to obtain the dense samples out of these powders and to compare the results with theoretical model. The applied pressure was between 20 and 45 MPa and process duration from 5 up to 30 min. It was found that the model did not provide reliable results in this range of pressures, temperatures and Al_2O_3 powder dimensions. In general, experiments provided much higher densification rate than that calculated, so it was necessary to modify the model.

2.2 Initial Stage of Densification

It is widely admitted that the origin of the ultra-rapid densification in the electrical field is still controversial [12]. It is known that various mass transfer mechanisms depend significantly on the temperature, pressure, and certain dimensions of the diffusion ways. Especially, it is important to consider a linear dimension for nanosize powders hot-pressing, where diffusion processes play the key role in the mass transfer [13]. Moreover, under the outer electrical field, e.g. during spark plasma sintering, diffusion coefficients considerably increase [14, 15]. It can be assumed that in the first stage of densification, when relative density is $D_{R0} < D_R < 0.9$, initially spherical particles join together increasing number of contacts with intensely growing neck radiuses. Around a fixed particle center of initial radius R, other particles are joining causing the growth of a solidified particle and increase of its radius to the new dimension R'. The formulas derived from the Ashby's model [8, 9] in application to this particular case, can be presented as follows:

$$R' = \left(\frac{D_R}{D_{R0}}\right)^{1/3} R, \tag{1}$$

where D_{R0} and D_R are initial and actual density, respectively. For the random compaction of the particles in the powder, it can be assumed $D_{R0} = 0.64$.

When the spherical particle grows, coalescence of two spheres takes place by surface diffusion. As the distance between their two centers decrease, the interconnection volume between two spheres can be calculated and redistributed to the empty spaces. At the same time, neck radiuses increase and new contacts between particles are initiated increasing their number Z. Dependence between the number of contacts with neighboring spheres Z and the relative density D_R can be written as follows:

$$Z = 12 D_R, \tag{2}$$

In fact, number of contacts Z increases from 7.7 at the beginning of hot isostatic pressing, when relative density of the loose powder is $D_{R0} = 0.64$, up to $Z = 12$ when the full density $D_R = 1$ is reached. Average contact surface s_c can be calculated from the following equation:

$$s_c = \frac{\pi}{3} \frac{(D_R - D_{R0})}{(1 - D_{R0})} R^2, \tag{3}$$

The radius of the neck r_n is dependent on the relative density D_R, and this dependency can be expressed as follows:

$$r_n = \sqrt{\frac{s_c}{\pi}} = \frac{1}{\sqrt{3}} \left(\frac{D_R - D_{R0}}{1 - D_{R0}}\right)^{1/2} R. \tag{4}$$

On the other hand, the curvature radius of the neck γ_n can be calculated as follows:

$$\gamma_n = \frac{r_n^2}{2(R - r_n)} \cong R(D_R - D_{R0}). \tag{5}$$

Under the outer pressure P, contact areas between particles are subject to the force f, which in average can be calculated as follows:

$$f = \frac{4\pi R^2}{Z}P. \tag{6}$$

Hence, effective pressure P' in each point can be determined from the following equation:

$$P' = \frac{f}{s_c} = \frac{(1 - D_{R0})}{D_R^2(D_R - D_{R0})}P. \tag{7}$$

It can be noted that P' would be close to P when D_R is close to 1, i.e. when the full theoretical density is reached.

However, during the second stage of the sintering process, when $0.9 < D_R < 1$, the empty spaces are trapped between the particles and form closed pores. It can be assumed that the pores are distributed in the corners of the polyhedron-form particles. Radius of the pores r_p can be calculated as follows:

$$r_p = \left(\frac{1 - D_R}{6}\right)^{1/3} R. \tag{8}$$

The closure of the pores poses a problem with their inner pressure P_i, which prevents sintered material from reaching its full theoretical density. The inner pressure can be calculated as follows:

$$P_i = P_0\frac{(1 - D_{RC})D_R}{(1 - D_R)D_{RC}}, \tag{9}$$

where P_0 is the air pressure in the pores at the closure moment, and D_{RC} is a critical value of relative density that corresponds with the pores closure.

2.3 Relative Density Summation

In the model, three densification mechanisms were considered, namely plastic deformation, diffusion and creep. Summation of all these phenomena provides overall understanding of the relative density rate.

Plastic deformation works after certain pressure $P' > 3\sigma_f$ is reached, where σ_f is the flow stress of the material. Simultaneously, the contact area between particles is growing. In the first stage of sintering, densification promoted by plastic deformation can be described by the following equation:

$$D_{Rpl} = \left(\frac{(1 - D_{R0})P}{1.3\sigma_f} + D_{R0}^3\right), \tag{10}$$

where D_{Rpl} is the relative density generated by plastic deformation. However, in the second stage of sintering, D_{Rpl} is described by other equation:

$$D_{Rpl} = 1 - \exp\left(-\frac{3}{2}\frac{P}{\sigma_f}\right). \tag{11}$$

In the cases of *diffusion* and *creep* mechanisms, it was found convenient to describe them using densification rates $\dot{D}_{R1}$ and $\dot{D}_{R2}$, respectively. Again, diffusion rate during the first stage of sintering is calculated differently from the one during the second stage. In the first stage, mass transfer tales place from the contact zones between powder particles towards the neck formed due to the grain-boundary and volume diffusion. Thus, in the first stage, diffusion-promoted densification rate $\dot{D}_{R1}$ can be calculated as follows:

$$\dot{D}_{R1} = \frac{43(1 - D_{R0})^2}{(D_R - D_{R0})^2} \frac{(\delta D_b - \gamma_n D_v)}{kTR^3} \Omega P, \tag{12}$$

where D_v and D_b are the diffusion coefficients by volume and by grain-boundaries, respectively, δ is the effective thickness of a grain boundary, k is the Boltzmann constant, T is the absolute temperature, and Ω is the atomic volume. However, in the second stage of the sintering process, it should be calculated from different formula, considering radiuses of pores r_p instead of radiuses of necks γ_n:

$$\dot{D}_{R1} = 54 \frac{\Omega(\delta D_b - r_p D_v)}{kTR^3} P \sqrt[5]{1 - D_R}. \tag{13}$$

Generally, creep can be described by the following formula:

$$\dot{\varepsilon} = \dot{\varepsilon}_0 \left(\frac{\sigma}{\sigma_0}\right)^n, \tag{14}$$

where $\dot{\varepsilon}$ is deformation rate, σ is the actual stress, while $\dot{\varepsilon}_0$, σ_0, and n are the parameters of the particular material.

However, two types of creep should be distinguished in the model. It is a deformation-promoted creep with related densification rate $\dot{D}_{R2}$ in the areas of contact between the particles, on one hand, and Nabarro-Herring and Coble creep with distinctive densification rate $\dot{D}_{R3}$, on the other hand. Both types should be calculated differently in the first and the second stages of the sintering process.

The densification rate $\dot{D}_{R2}$ related to the first type of creep in the first stage of sintering, when relative density is below 0.9, can be calculated as follows:

$$\dot{D}_{R2} = \frac{3}{2}\left(\frac{\dot{\varepsilon}_0}{\sigma_0^n}\right) \frac{D_R(1 - D_R)}{(1 - [1 - D_R]^{1/n})^n} \left(\frac{3}{2n}P\right)^n. \tag{15}$$

However, when the relative density is above 0.9 and is approaching 1, densification rate should be calculated as follows:

$$\dot{D}_{R2} = 5.3\left(D_R^2 D_{R0}\right)^{1/3} \frac{r_n}{R} \left(\frac{\dot{\varepsilon}_0}{\sigma_0^n}\right) \left(\frac{P'}{3}\right)^n. \tag{16}$$

On other hand, Nabarro-Herring and Coble creep mechanisms appear in the lowest stress range [16]. They cannot occur in monocrystalline powder particles without grain boundaries, and thus, are typical for the pressure-assisted sintering mechanism [17]. These mechanisms take place when the grain dimensions are substantially smaller than that of powder particles. During the first stage of sintering process, the following formula

can be applied to calculate densification rate $\dot{D}_{R3}$ related to the Nabarro-Herring and Coble creep mechanisms:

$$\dot{D}_{R3} = 24.9 \frac{\Omega}{kT\overline{G}^2} \left(D_R^2 D_{R0}\right)^{1/3} \frac{r_n}{R} \left(D_v + \frac{\pi \delta D_b}{\overline{G}}\right) P', \tag{17}$$

where $\overline{G}$ is an average grain size. However, when the relative density is above 0.9 and is approaching 1, densification rate $\dot{D}_{R3}$ should be calculated as follows:

$$\dot{D}_{R3} = 31.5 \frac{\Omega}{kT\overline{G}^2} (1 - D_R)^{1/3} \frac{r_n}{R} \left(D_v + \frac{\pi \delta D_b}{\overline{G}}\right) P. \tag{18}$$

Finally, the relative density can be obtain from the summation of the partial densification promoted by plastic deformation and the three respective densification rates multiplied by the pressing time t, as follows:

$$D_R = D_{Rpl} + \sum_{i=1}^{3} \dot{D}_{Ri} t. \tag{19}$$

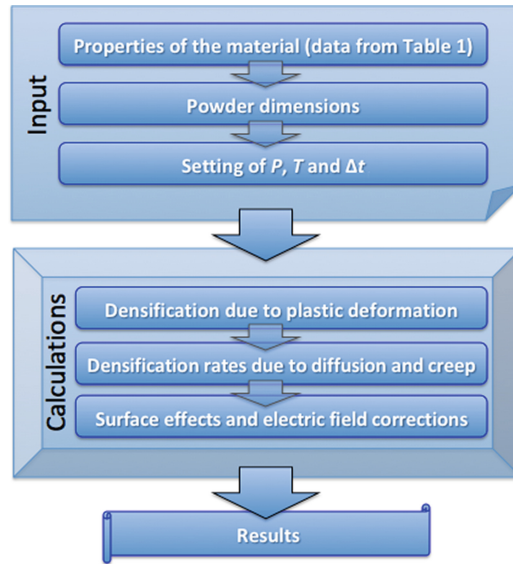## 2.4   Algorithm for Alumina Powder Calculations

In order to plot the diagrams for densification during hot isostatic pressing of alumina, the main physical data related to the sintering process were taken from literature [18] and given in Table 1.

Table 1. Chosen physical and mechanical properties of Al_2O_3.

	Property, units	Value
1	Atomic volume, Ω (m^3)	$4.25 \cdot 10^{-29}$
2	Burgers vector, b (m)	$4.76 \cdot 10^{-10}$
3	Melting point, T_m (K)	2320
4	Flow stress, σ_f (MPa)	1500
5	Shear modulus at 300 K, μ_0 (MPa)	$0.24 \cdot 10^4$
6	Ratio $\frac{T_m d\mu}{\mu_0 dT}$	-0.35
7	Volume diffusion, D_{0v} (m^2/s)	$2.8 \cdot 10^{-10}$
8	Grain-boundary diffusion, δD_{0b} (m^3/s)	$8.6 \cdot 10^{-10}$

Based on the data from Table 1 and the equations from (1) to (19), the alumina powder densification process under directly applied electrical current was simulated. The calculation algorithm is presented in Fig. 1.

Apart from the equations from (1) to (19), it was found necessary to introduce corrections. Some effect on the final results may have contaminations on the surface of the

Fig. 1. Algorithm of calculation of alumina sintered sample relative density under directly applied electric current.

powder particles, as well as their difference from the spherical form and non-uniform dimensions. Some corrective coefficients were introduced, accordingly. Moreover, deviations of the electric field from the theoretical values also were taken into consideration in the calculations.

3   Experimental Verification

To verify the model, several experiments were performed using the equipment for field activated sintering [19]. Time and resources constrains did not allow for full statistical verification, but interesting initial results were obtained for different pressures. Both experimental results and theoretical data are shown in Figs. 2, 3 and 4, where colored plots correspond with calculations, and black points represent experimental data.

In Fig. 2, there is a plot of theoretical relative density for different sintering temperatures, calculated for the pressure 20 MPa. In accordance with expectations, the model shows that higher density can be obtained at certain temperature when the holding time is longer. It is noteworthy, however, that the time $t = 5$ min provided almost linear function $D_R = f(T)$. Since 20 MPa is rather rarely used pressure, only one experiment was performed for this value of P at temperature 1290 °C. The relative density $D_R = 0.84$ was obtained, which was much closer to the theoretical value for 1 min (0.83) than that for 5 min (0.90).

Nevertheless, difference of 7% between theoretical and experimental values for the temperature 1290 °C at pressure $P = 20$ MPa and pressing time 5 min can be considered satisfactory.
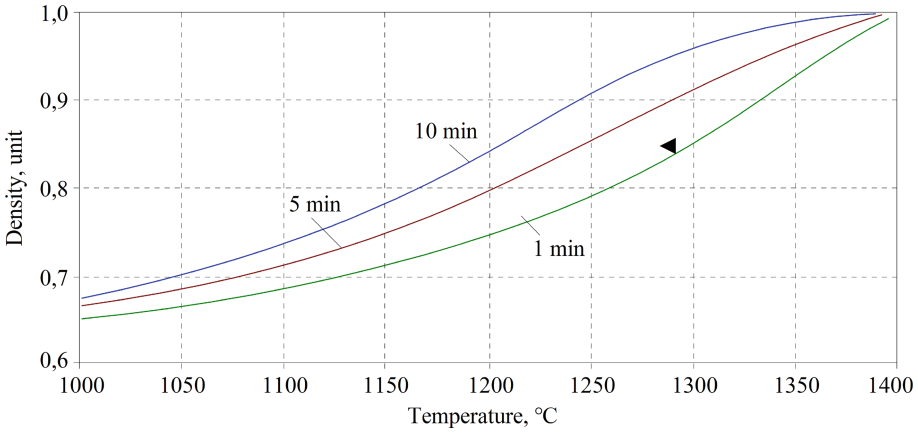
Fig. 2. Theoretical relative density of Al_2O_3 powder with particles diameter 0.6 μm at pressure $P = 20$ MPa calculated for different temperatures. Experimental result: ◄– $P = 20$ MPa, $T = 1290$ °C, $t = 5$ min, $D_R = 0.84$.

Figure 3 presents a graph of theoretical relative density for different sintering temperatures, calculated for the pressure 45 MPa. It should be noted that the general trend is the same as for 20 MPa (Fig. 2), but the curve corresponding with holding time $t = 5$ min exhibited less linearity. At the temperatures above 1300 °C, increase of density is smaller.
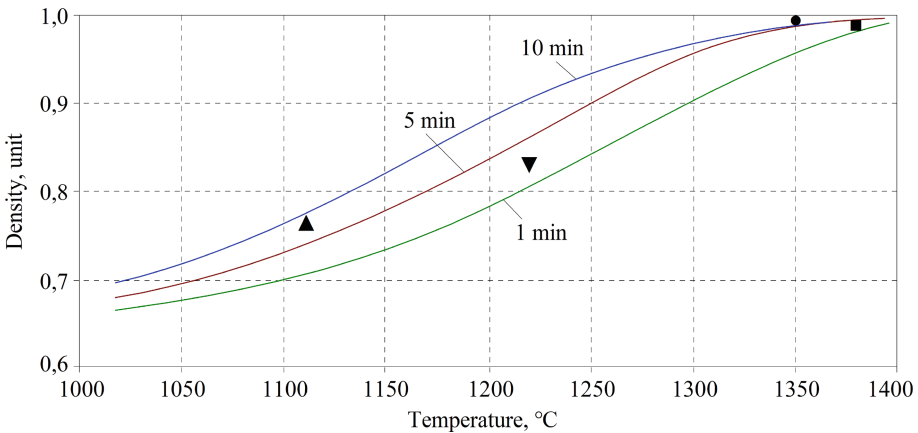

Fig. 3. Theoretical relations between relative density of hot-pressed Al_2O_3 powder (particles diameter 0.6 μm) and sintering temperature at the pressure $P = 45$ MPa, and experimental results for pressing time 5 min: ▲– at temperature 1110 °C, obtained relative density $D_R = 0.766$; ▼– at 1220 °C, $D_R = 0.83$; ● – at 1350 °C, $D_R = 0.999$; ■– at 1380 °C, $D_R = 0.999$.

Important characteristic can be derived from the Fig. 3 is that at temperature 1330 °C, the relative density obtained after 5 min will not improve after 10 min. In fact, no substantial improvement can be achieved also through further increase of the temperature, since experimental $D_R = 0.999$ was obtained both at 1350 °C and at 1380 °C.

In the case of lower sintering temperatures, experimental results exhibited good conformity with the theoretical model. The difference was less than ±4% between experimental and calculated relative densities D_R.

Keeping in mind that the nanopowders could provide more dense material and nanostructural ceramics posses better characteristics than the microstructural ones [20], additional experiment was performed with alumina nanopowder. The particle dimensions were 0.06 μm, which theoretically was expected to provide much higher relative density at the same temperatures and holding times, as it can be seen in Fig. 4. The experimental point of $D_R = 0.999$ was obtained after 5 min of sintering at the temperature 1250 °C.
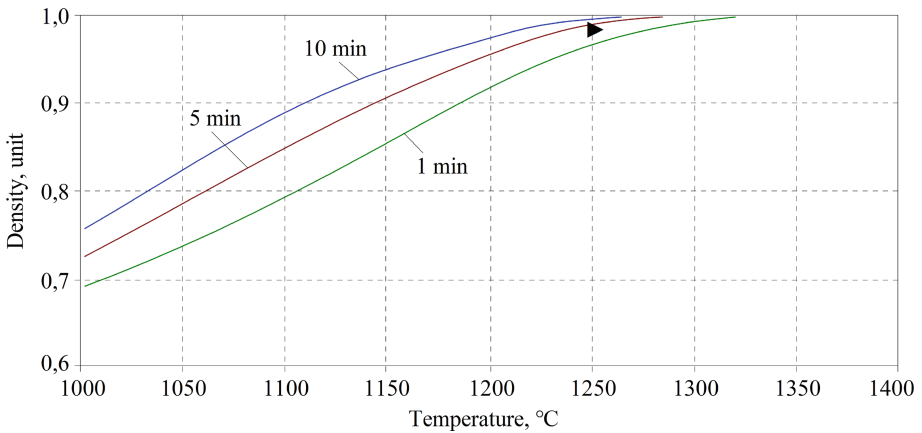
Fig. 4. Theoretical relative density of Al_2O_3 nanopowder with particles diameter 0.06 μm at pressure $P = 45$ MPa calculated for different temperatures. Experimental: ▶– $P = 45$ MPa, $T = 1250$ °C, $t = 5$ min, $D_R = 0.999$.

From the practical perspective, these results are enough to confirm the fidelity of the proposed model. It makes possible to estimate the temperature and holding time for the alumina powder, and to obtain required relative density with accuracy below 5% for higher pressures. It is planned to perform further investigations on repeatability of the densification process parameters and resulting density, and to introduce necessary corrections to the model.

4   Conclusions

From the performed theoretical analysis of the hot-pressing process under directly applied electrical current it can be concluded that differentiation between several densification mechanisms is crucial. In particular, plastic deformation, diffusion and creep of

two kinds should be summed up when calculating the relative density of sintered specimen. Moreover, from the practical perspective, division of a sintering process to two stages and application of proper equations for each of them provided good estimation without necessity of distinguishing more stages.

Experimental results initially confirmed the correctness of the model. At lower pressure $P = 20$ MPa, difference between the experiment and the model was 7%, while at $P = 45$ MPa experimental results differed from the model by no more than $\pm 4\%$. Experiments also confirmed the theoretical prediction that at pressure $P = 45$ MPa the highest relative density can be obtained at 1350 °C after holding time $t = 5$ min, with no necessity of temperature increase or process prolongation. Additional experiments with alumina nanopowder with particles diameter 0.06 µm demonstrated possibility of full densification even at lower temperature of 1250 °C, in conformity with the theoretical model.

It is necessary, however, to perform more experiments in order to check the accuracy of the model. In particular, statistical analysis of the repeatability should be done, as well as other sintered materials should be considered. Nevertheless, from the practical perspective, the model can be applied for estimation of the process parameters to obtain the desired density of sintered alumina.

References

1. Abedi, M., Asadi, A., Vorotilo, S., Mukasyan, A.S.: A critical review on spark plasma sintering of copper and its alloys J. Mater. Sci. **56**(36), 19739–19766 (2021). https://doi.org/10.1007/s10853-021-06556-z

2. Munir, Z.A., Quach, D.V., Ohyanagi, M.: Electric field and current effects on sintering. In: Castro, R., van Benthem, K. (eds.) Sintering, pp. 137–158. Springer, Berlin, Heidelberg (2012). https://doi.org/10.1007/978-3-642-31009-6_7

3. Anselmi-Tamburini, U., Spinolo, G., Maglia, F., Tredici, I., Holland, T.B., Mukherjee, A.K.: Field Assisted Sintering Mechanisms. In: Castro, R., van Benthem, K. (eds.) Sintering, pp. 159–193. Springer, Berlin, Heidelberg (2012). https://doi.org/10.1007/978-3-642-31009-6_8

4. Swenson, O.F., Marinov, V.: Laser processing of direct-write nano-sized materials. In: Lawrence, J. (ed.), Advances in Laser Materials Processing. 2nd edn., pp. 571–594. Woodhead Publishing, Duxford, UK (2018). https://doi.org/10.1016/B978-0-08-101252-9.00019-4D.S

5. Yang, H., et al.: Unveiling exceptional sinterability of ultrafine α-Al$_2$O$_3$ nanopowders. J. Materiomics 7 4 837 844 https://doi.org/10.1016/j.jmat.2020.12.011

6. Sánchez-González, E., Miranda, P., Meléndez-Martínez, J.J., Guiberteau, F., Pajares, A.: Temperature dependence of mechanical properties of alumina up to the onset of creep. J. Eur. Ceram. Soc. **27**(11), 3345–3349 (2007). https://doi.org/10.1016/j.jeurceramsoc.2007.02.191

7. Sirota, V.V., Gevorkyan, E.S., Kovaleva, M.G., Ivanisenko, V.V.: Structure and properties of nanoporous ceramic Al2O3 obtained by isostatic pressing. Glass Ceramics (Engl. Transl. Steklo i Keramika) **69**(9–10) 342–345 (2013)

8. Wilkinson, D.S., Ashby, M.F.: Pressure sintering by power law creep. Acta Metall. **23**(11), 1277–1285 (1975). https://doi.org/10.1016/0001-6160(75)90136-4

9. Swinkels, F.B., Ashby, M.F.: A second report on sintering diagrams. Acta Metall. **29**(2), 259–281 (1981). https://doi.org/10.1016/0001-6160(81)90154-1

10. Wakai, F., Guillon, O., Okuma, G., Nishiyama, N.: Sintering forces acting among particles during sintering by grain-boundary/surface diffusion. J. Am. Ceram. Soc. **102**(2), 538–547 (2019)

11. De Jonghe, L.C., Rahaman, M.N.: Sintering of Ceramics. In: Somiya, S. et al. (eds.), Handbook of Advanced Ceramics, pp. 187–264, Elsevier, Amsterdam (2003)

12. Biesuz, M., Sglavo, V.M.: Electric forces effect on field-assisted sintering. J. Eur. Ceram. Soc. **40**(15), 6259–6265 (2020). https://doi.org/10.1016/j.jeurceramsoc.2020.06.069

13. Skorokhod, V.V., Uvarov, I.V., Ragulya, A.V.: Physico-chemical kinetics in the nanostructured systems. Akademperiodica, Kyiv (2001). (in Russian)

14. Raychenko, A.I.: Fundamentals of the process of sintering powders by passing electric current. Metalurgia, Moskva (1987). (in Russian)

15. Tamura, Y., Zapata-Solvas, E., Moshtaghioun, B.M., Gómez-García, D., Domínguez-Rodríguez, A.: Grain-boundary diffusion coefficient in α-Al2O3 from spark plasma sintering tests: evidence of collective motion of charge disconnections. Ceram. Int. **44**(15), 19044–19048 (2018). https://doi.org/10.1016/j.ceramint.2018.07.073

16. Maruyama, K.: Fundamental aspects of creep deformation and deformation mechanism map. In: Abe, F., Kern, T.U., Viswanathan, R. (eds.) Creep-Resistant Steels, pp. 265–278, Woodhead Publishing, Cambridge, UK (2008). https://doi.org/10.1533/9781845694012.2.265

17. Trapp, J., Semenov, A., Nöthe, M., Wallmersperger, T., Kieback, B.: Fundamental principles of spark plasma sintering of metals: part III – densification by plasticity and creep deformation. Powder Metall. **63**(5), 329–337 (2020). https://doi.org/10.1080/00325899.2020.1834748

18. Kislyi, P.S., Bodnaruk, N.N., Gorichok, N.I., Zaverukha, O.V., Kryl, Y.A, Kuzenkova, M.A.: Physicochemical fundamentals of the manufacturing of refractory superhard materials. Naukova Dumka, Kyiv (1986). (in Russian)

19. Gevorkyan, E., Lavrynenko, S., Rucki, M., Siemiątkowski, Z., Kislitsa, M.: Preparation of nanostructured materials by electrical sintering. In: Proceedings of the 7th International Conference on Mechanics and Materials in Design (M2D2017), pp. 663–666. Albufeira/Portugal (2017)

20. Gevorkyan, E., et al.: Sintered nanocomposites ZrO2-WC obtained with field assisted hot pressing. Compos. Struct. **259** 113443 (2021). https://doi.org/10.1016/j.compstruct.2020.113443